




Targeting HIF-1 α by newly synthesized Indolephenoxyacetamide (IPA) analogs to induce anti-angiogenesis-mediated solid tumor suppression

Fares Hezam Al-Ostoot^{1,2} · Ankith Sherapura³ · Vigneshwaran V^{3,4} · Giridhara Basappa³ · Vivek H.K.⁵ · Prabhakar B. T³ · Shaukath Ara Khanum¹ 

Received: 2 February 2021 / Revised: 8 April 2021 / Accepted: 10 April 2021 / Published online: 26 April 2021
© Maj Institute of Pharmacology Polish Academy of Sciences 2021

Abstract

Background Hypoxic microenvironment is a common feature of solid tumors, which leads to the promotion of cancer. The transcription factor, HIF-1 α , expressed under hypoxic conditions stimulates tumor angiogenesis, favoring HIF-1 α as a promising anticancer agent. On the other hand, synthetic Indolephenoxyacetamide derivatives are known for their pharmacological potentiality. With this background here, we have synthesized, characterized, and validated the new **IPA (8a–n)** analogs for anti-tumor activity.

Methods The new series of **IPA (8a–n)** were synthesized through a multi-step reaction sequence and characterized based on the different spectroscopic analysis FT-IR, ¹H, ¹³C NMR, mass spectra, and elemental analyses. Cell-based screening of **IPA (8a–n)** was assessed by MTT assay. Anti-angiogenic efficacy of **IPA (8k)** validated through CAM, Rat corneal, tube formation and migration assay. The underlying molecular mechanism is validated through zymogram and IB studies. The in vivo anti-tumor activity was measured in the DLA solid tumor model.

Results Screening for anti-proliferative studies inferred, **IPA (8k)** is a lead molecule with an IC₅₀ value of -5 μ M. Anti-angiogenic assays revealed the angiopreventive activity through inhibition of HIF-1 α and modulation downstream regulatory genes, VEGF, MMPs, and P53. The results are confirmative in an in vivo solid tumor model.

B.T. Prabhakar and Shaukath Ara Khanum contributed equally.

✉ Prabhakar B.T
prabhakarbt1@kussc.org

✉ Shaukath Ara Khanum
shaukathah@ycm.uni-mysore.ac.in

¹ Present Address: Department of Chemistry, Yuvaraja's College, University of Mysore, Mysuru, India

² Department of Biochemistry, Faculty of Education and Science, Al-Baydha University, Mecca, Yemen

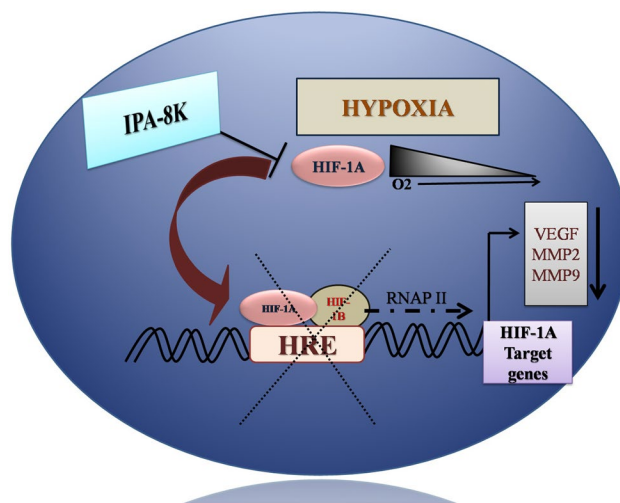
³ Molecular Biomedicine Laboratory, Postgraduate Department of Studies and Research in Biotechnology, Sahyadri Science College, Kuvempu University, Shivamogga, Karnataka, India

⁴ Present Address: Department of Pharmacology, University of Illinois at Chicago, Chicago, USA

⁵ Faculty of Natural Sciences, Adichunchanagiri University-Center for Research and Innovation, Adichunchanagiri University, BGSIT Campus, B.G. Nagara, Mandya, Karnataka 571448, India

Conclusion The IPA (8k) is a potent anti-proliferative molecule with anti-angiogenic activity and specifically targets HIF1 α , thereby modulates its downstream regulatory genes both in vitro and in vivo. The study provides scope for new target-specific drug development against HIF-1 α for the treatment of solid tumors.

Graphic abstract



Keywords Indolephenoxyacetamide · Angiogenesis · HIF-1 α · Solid tumor

Introduction

Angiogenesis is a complex and multistep process stimulated by various biological signals regardless of its physiological or pathological action. Many proangiogenic factors including VEGF are activated in response to signals leading to damage in blood vessels, infarction, and reduction in the flow of blood that lead to a decrease in the supply of oxygen [1]. The condition is termed as hypoxia, which mediates angiogenesis, invasion and, metastasis in most of the solid tumors and creates indulgence for all the cancer cells with respect to adequate oxygenation [3]. The hypoxic microenvironment triggers the angiogenic process by stimulating proangiogenic factors triggered by the upstream signaling cascade, led by the overexpression of the transcription factor hypoxia-inducible factor (HIF)-1 α [2].

Highly stabilized HIF-1 α involved in the tolerance of tumor cells to a hypoxic environment, translocates into the nucleus and forms heterodimer, thereby regulating oxygen concentration which is tightly associated in the pathophysiology of solid tumors [4]. This results in the activation of the tumor-promoting proangiogenic genes, such as VEGF, MMPs and angiopoietins, etc. Overexpression of HIF-1 α , significantly promotes aggressive angiogenesis-mediated tumorigenesis, contributing

to a specific interest in HIF-1 α targeted therapy [5]. Therefore, developing novel molecules that specifically counteract tumor cell growth with target specificity and spread potency is critical for the treatment of angiogenic-dependent neoplasia.

The heterocyclic structures are deemed to be significantly useful to medicinal chemists in that they offer a real break to the designing and establishment of one library depending on a specific central scaffold and then assess it against several target receptors [6]. In indole medications, being rich with electrons in pyrole moiety along with other qualities can utilize the non-covalent interactions with many other molecules by creating hydrogen bonding in the NH group using the π - π system and is considered a privileged scaffold in pharmaceutical research and drug development [7], such as anti-oxidant [8], anti-microbial [9], anti-HIV [10] and anti-cancer [11]. In particular, some indoles have been found to constrain the growth of several cancers along with boosting apoptosis and stopping tumor invasion and metastasis [12]. With this rationale, the investigation of new indole analogs carrying acetamide moiety can improve and also display a pleasing variety of biological effects against a diversity of health issues [13]. As an approach, in the current investigation, new series of substituted phenoxy acetic acids bonded at the ortho position of diamino benzene which then conjugated to potent indole acids backbone have been synthesized and evaluated for potential anti-cancer activity. Studies

of the structure–activity relationship (SAR) have shown that the substituents of halogen at para position influence the activity of the indole derivatives with significant anti-angiogenesis-mediated anti-cancer activity.

Materials and methods

Experimental section

The chemicals, solvents, and reagents were procured from Sigma Aldrich Chemicals Pvt. Ltd. with 90–99% purity. Using the instrument Chemi Line CL-725 Micro-controller-based melting point and boiling point with a digital thermometer, the melting points and boiling point were determined. The progress and completion of reactions were monitored using thin-layer chromatography (TLC) performed on aluminium-backed silica plates and the spots were detected using UV lamp at $\lambda = 254$ nm. The IR spectra were recorded by the potassium bromide pellet method on Cary 630 FTIR Agilent spectrophotometer. The NMR (^1H and ^{13}C) spectra were recorded on a VNMR-400, 100 MHz Agilent-NMR spectrophotometer in DMSO and mass spectra were obtained on Mass Lynx SCN781 spectrometer TOF mode. Elemental analysis was obtained using Thermo Finnigan Flash EA 1112 CHN analyser and the findings are within $\pm 0.4\%$ of the calculated value.

Chemistry

General procedure for the synthesis of phenoxy ester analogs (3a–h)

To the solution of substituted phenols (**1a–h**, 0.080 mol) and ethyl chloroacetate (**2**, 0.080 mol) in dry acetone (25 ml), anhydrous potassium carbonate (0.075 mol) is added and the reaction mixture was refluxed for 10–12 h. The mixture was then allowed to cool at room temperature and the solvent was removed by distillation. The residual mass was triturated with cold water to remove potassium carbonate, and the product was extracted with ether (3×25 ml). The ether layer was washed with a 10% sodium hydroxide solution (3×25 ml) followed by water (3×25 ml) and dried over anhydrous sodium sulfate, then the solvent was evaporated to afford compounds (**3a–h**). Finally, compounds (**3a–h**) were purified by the distillation method [14].

General procedure for the synthesis of phenoxyacetic acid analogs (4a–h)

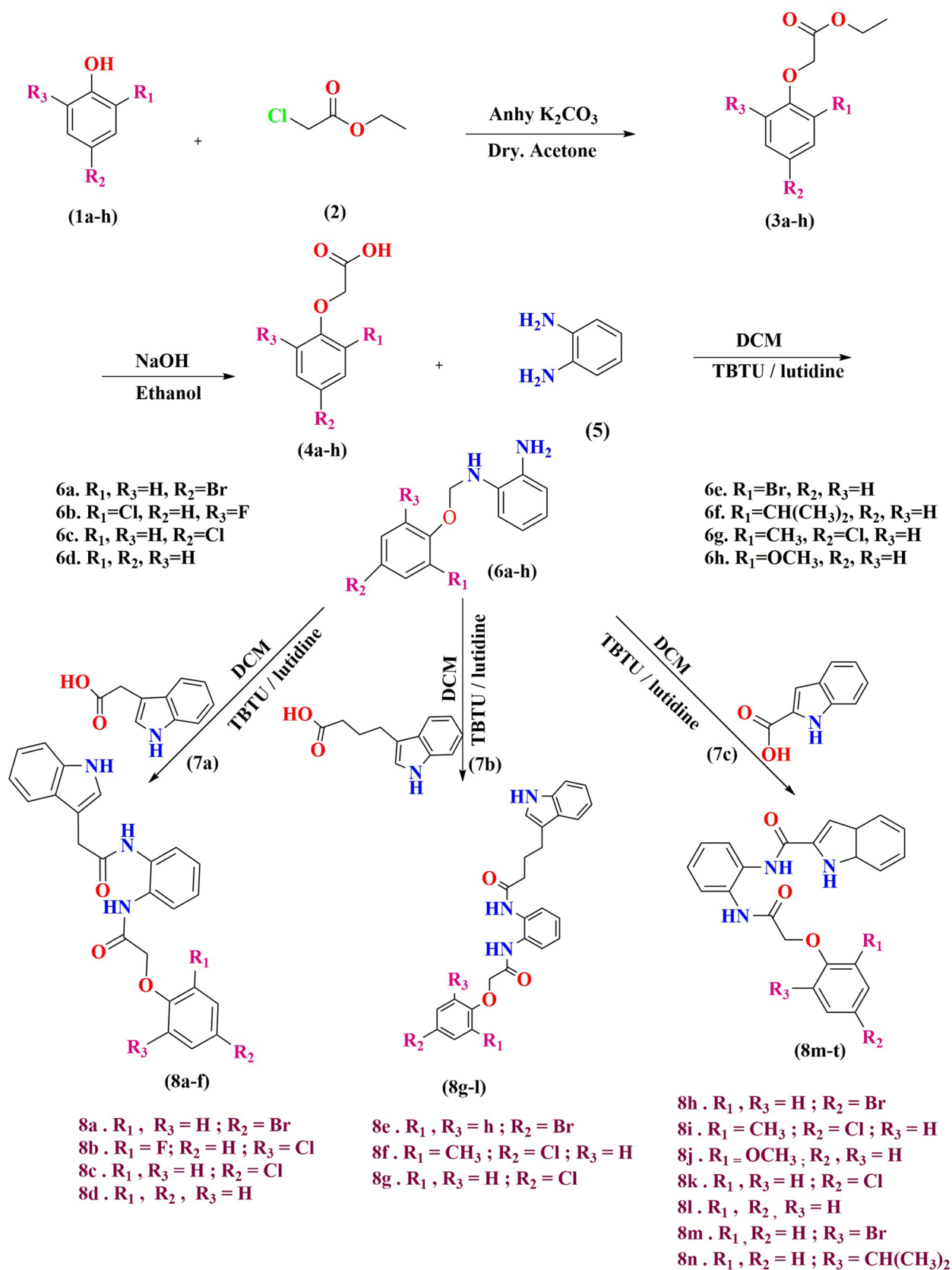
To the solution of compounds (**3a–h**, 0.05 mol) in ethanol (15 ml), alcoholic sodium hydroxide solution (3 ml, 0.04 mol) was added. The reaction mixture was allowed to reflux for 8–10 h, and the completion of the reaction was monitored using TLC hexane: ethyl acetate: methanol system (6:3:1). The mixture was cooled and acidified with 2 N hydrochloric acid. The precipitate was filtered, washed with distilled water, and finally recrystallized from methanol to afford desired compounds (**4a–h**) [15].

General procedure for the synthesis of *N*-(2-Amino-phenyl)-2-phenoxy-acetamide analogs (6a–h)

The syntheses of compounds of *N*-(2-aminophenyl)-2-phenoxyacetamide analogs (**6a–h**), were accomplished using the condensation procedure. To a solution of (**4a–h**, 0.009 mol), in dry dichloromethane (DCM) (10 ml), lutidine (1.3 vol.) was added, followed by the addition of *o*-phenylenediamine (**5**, 0.009 mol), the mixture was stirred at room temperature for 30 min. The reaction mixture was cooled to 0–5 °C, TBTU (0.02 mol) was added, over a period for 30 min while maintaining the temperature below 5 °C. The reaction was allowed to stir overnight. After completion of the reaction which was monitored by TLC using a mobile-phase system [hexane: ethyl acetate (3:1)], the mixture was diluted with 20 ml of DCM and treated with 2 N hydrochloric acid solution (20 ml). The organic layer was washed with water (3×25 ml) and brine (3×25 ml). Finally, the organic layer was dried over anhydrous sodium sulfate and concentrated to afford compounds (**6a–h**).

General procedure for the synthesis of indolephenoxyacetamid analogs IPA (8a–n)

To the solution of compounds (**6a–h**, 0.002 mol), in dry DCM (10 ml), the (1*H*-Indol-3-yl)-acetic acid, 4-(1*H*-indol-3-yl) butanoic acid, and 1*H*-indole-2-carboxylic acid (**7a–c**, 0.002 mol) were added at room temperature followed by the addition of lutidine (0.002 mol). The reaction mixture was stirred for 30 min and the mixture was cooled to 0–5 °C, then, the TBTU (0.003 mol) was added over a period for half an hour while maintaining the temperature between 0 and 5 °C. The reaction was stirred overnight and monitored by TLC using hexane and ethyl acetate (3:1) system. The reaction mixture was diluted with (20 ml) of DCM and treated with 10% of sodium bicarbonate solution (3×25 ml). The organic layer was washed with water (3×25 ml), dried over anhydrous sodium sulfate, and concentrated to yield the title compounds **IPA (8a–n)**. The



Scheme 1 Reaction pathway for the synthesis of the title compounds IPA (8a–n)

schematic representation of the synthesized compounds **IPA (8a–n)** is shown in Scheme 1.

Synthesis of **N-[2-(2-1H-Indol-3-yl-acetylamino)-phenyl]-2-phenoxyacetamide analogs IPA (8a–d)**

N-(2-(2-(1H-indol-3-yl)acetamido)phenyl)-2-(4-bromophenoxy)acetamide (8a)

Yield: 79%; M.P. 186–188 °C; FT-IR (KBr, ν_{\max} cm⁻¹): 1635 (amide, C=O), 3215–3325 (amide CO–NH). ¹H NMR (400 MHz, DMSO-d₆) δ (ppm): 3.70 (s, 2H, CH₂), 4.45 (s, 2H, OCH₂), 6.85–7.60 (m, 13H, Ar–H), 9.55 (s, 1H, NH), 9.65 (s, 1H, NH), 10.88 (s, 1H, NH indole); ¹³C NMR (DMSO-d₆) δ : 171.07, 167.04, 157.82, 136.63, 131.16, 130.57, 129.95, 127.61, 125.85, 125.73, 125.55, 125.32, 124.63, 121.84, 121.47, 118.91, 115.16, 111.87, 108.36, 67.35, 33.52; LC–MS m/z 477 [M+], 479 [M+2]. Anal. Calcd. for C₂₄H₂₀BrN₃O₃(477): C, 60.26; H, 4.21; N, 8.78. Found: C, 60.20; H, 3.95; N, 8.74%.

2-(2-Chloro-6-fluoro-phenoxy)-N-[2-(2-1H-indol-3-yl-acetylamino)-phenyl]acetamide (8b)

Yield: 81%; M.P. 187–190 °C; FT-IR (KBr, ν_{\max} cm⁻¹): 1630 (amide, C=O), 3220–3320 (amide CO–NH). ¹H NMR (400 MHz, DMSO-d₆) δ (ppm): 3.66 (s, 2H, CH₂), 4.47 (s, 2H, OCH₂), 6.80–7.85 (m, 12H, Ar–H), 9.53 (s, 1H, NH), 9.66 (s, 1H, NH), 10.76 (s, 1H, NH indole); ¹³C NMR (DMSO-d₆) δ : 172.05, 167.03, 157.81, 136.65, 131.15, 130.57, 129.93, 127.65, 125.83, 125.70, 125.54, 125.33, 124.63, 121.84, 121.46, 118.91, 114.16, 110.87, 108.36, 67.35, 33.50; LC–MS m/z 451 [M+], 453 [M+2]. Anal. Calcd. for C₂₄H₁₉ClFN₃O₃(451): C, 63.79; H, 4.24; N, 9.30. Found: C, 63.66; H, 4.18; N, 9.25%.

2-(4-Chloro-phenoxy)-N-[2-(2-1H-indol-3-yl-acetylamino)-phenyl]acetamide (8c)

Yield: 78%; M.P. 174–177 °C; FT-IR (KBr, ν_{\max} cm⁻¹): 1640 (amide, C=O), 3212–3322 (amide CO–NH). ¹H NMR (400 MHz, DMSO-d₆) δ (ppm): 3.72 (s, 2H, CH₂), 4.45 (s, 2H, OCH₂), 6.81–7.83 (m, 13H, Ar–H), 9.41 (s, 1H, NH), 9.68 (s, 1H, NH), 10.72 (s, 1H, NH indole); ¹³C NMR (DMSO-d₆) δ : 171.03, 167.05, 157.84, 136.63, 131.12, 130.55, 129.95, 127.65, 125.84, 125.71, 125.56, 125.32, 124.60, 121.86, 121.49, 118.91, 115.12, 110.87, 107.36, 67.35, 33.52; LC–MS m/z 433 [M+], 435 [M+2]. Anal. Calcd. for C₂₄H₂₀ClN₃O₃(433): C, 66.44; H, 4.65; N, 9.68. Found: C, 66.40; H, 4.60; N, 9.61%.

N-[2-(2-1H-Indol-3-yl-acetylamino)-phenyl]-2-phenoxyacetamide (8d)

Yield: 75%; M.P. 181–183 °C; FT-IR (KBr, ν_{\max} cm⁻¹): 1633 (amide, C=O), 3210–3320 (amide CO–NH). ¹H NMR (400 MHz, DMSO-d₆) δ (ppm): 3.70 (s, 2H, CH₂), 4.47 (s, 2H, OCH₂), 6.89–7.58 (m, 14H, Ar–H), 9.57 (s, 1H, NH), 9.68 (s, 1H, NH), 10.92 (s, 1H, NH indole); ¹³C NMR (DMSO-d₆) δ : 171.04, 167.07, 157.80, 136.65, 131.15, 130.59, 129.94, 127.62, 125.86, 125.76, 125.57, 125.30, 124.64, 121.81, 121.49, 118.90, 115.18, 111.86, 108.37, 67.33, 33.57; LC–MS m/z 400 [M+1]. Anal. Calcd. for C₂₄H₂₁N₃O₃(399): C, 72.16; H, 5.30; N, 10.52. Found: C, 72.10; H, 5.24; N, 10.47%.

Synthesis of **4-(1H-Indol-3-yl)-N-[2-(2-phenoxy-acetylamino)-phenyl]butyramide analogs IPA (8e–g)**

N-[2-[2-(4-Bromo-phenoxy)-acetylamino]-phenyl]-4-(1H-indol-3-yl)-butyramide (8e)

Yield: 76%; M.P. 176–178 °C; FT-IR (KBr, ν_{\max} cm⁻¹): 1635 (amide, C=O), 3210–3325 (amide CO–NH). ¹H NMR (400 MHz, DMSO-d₆) δ (ppm): 1.82 (m, 2H, CH₂), 2.33 (t, 2H, CO-CH₂), 2.51 (t, 2H, CH₂), 4.64 (s, 2H, OCH₂), 6.78–7.65 (m, 13H, Ar–H), 9.66 (s, 1H, NH), 9.75 (s, 1H, NH), 10.88 (s, 1H, NH indole); ¹³C NMR (DMSO-d₆) δ : 171.12, 168.03, 157.84, 136.60, 131.13, 130.51, 129.97, 127.61, 125.83, 125.71, 125.58, 125.32, 124.62, 121.84, 121.45, 118.90, 114.14, 111.88, 108.36, 67.35, 33.56, 25.28, 25.11; LC–MS m/z 505 [M+], 507 [M+2]. Anal. Calcd. for C₂₆H₂₄BrN₃O₃(505): C, 61.67; H, 4.78; N, 8.30. Found: C, 61.61; H, 4.72; N, 8.30%.

N-[2-[2-(4-Chloro-2-methyl-phenoxy)-acetylamino]-phenyl]-4-(1H-indol-3-yl)-butyramide (8f)

Yield: 78%; M.P. 186–188 °C; FT-IR (KBr, ν_{\max} cm⁻¹): 1635 (amide, C=O), 3215–3322 (amide CO–NH). ¹H NMR (400 MHz, DMSO-d₆) δ (ppm): 1.91 (m, 2H, CH₂), 2.40 (t, 2H, CO-CH₂), 2.53 (t, 2H, CH₂), 4.71 (s, 2H, OCH₂), 6.72–7.69 (m, 12H, Ar–H), 9.68 (s, 1H, NH), 9.79 (s, 1H, NH), 10.85 (s, 1H, NH indole); ¹³C NMR (DMSO-d₆) δ : 171.05, 167.03, 157.82, 136.62, 131.15, 130.55, 129.94, 127.60, 125.83, 125.71, 125.53, 125.30, 124.63, 121.84, 121.47, 118.91, 115.12, 111.83, 108.35, 67.35, 33.51, 25.25, 25.09, 16.34; LC–MS m/z 475 [M+], 477 [M+2]. Anal. Calcd. for C₂₇H₂₆ClN₃O₃(475): C, 68.13; H, 5.51; N, 8.83. Found: C, 68.02; H, 5.46; N, 8.80%.

***N*-{2-[2-(4-Chloro-phenoxy)-acetyl-amino]-phenyl}-4-(1*H*-indol-3-yl)-butyramide (8 g)**

Yield: 81%; M.P. 184–186 °C; FT-IR (KBr, ν_{\max} cm⁻¹): 1645 (amide, C=O), 3210–3330 (amide CO–NH). ¹H NMR (400 MHz, DMSO-*d*₆) δ (ppm): 1.65 (m, 2H, CH₂), 2.39 (t, 2H, CO–CH₂), 2.49 (t, 2H, CH₂), 4.71 (s, 2H, OCH₂), 6.63–7.69 (m, 13H, Ar–H), 9.11 (s, 1H, NH), 9.55 (s, 1H, NH), 10.91 (s, 1H, NH indole); ¹³C NMR (DMSO-*d*₆) δ : 171.07, 167.00, 157.83, 136.61, 131.19, 130.53, 129.95, 127.64, 125.84, 125.71, 125.56, 125.32, 124.60, 121.86, 121.50, 118.91, 115.20, 110.77, 107.35, 67.35, 33.51, 25.34, 25.19; LC–MS *m/z* 461 [M+], 463 [M+2]. Anal. Calcd. for C₂₆H₂₄ClN₃O₃ (461): C, 67.60; H, 5.24; N, 9.10. Found: C, 67.51; H, 5.18; N, 9.04%.

Synthesis of 1*H*-Indole-2-carboxylic acid [2-(2-phenoxy-acetyl-amino)-phenyl] amide analogs IPA (8 h-n)**1*H*-Indole-2-carboxylic acid****{2-[2-(4-bromo-phenoxy)-acetyl-amino]-phenyl}-amide (8 h)**

Yield: 88%; M.P. 176–178 °C; FT-IR (KBr, ν_{\max} cm⁻¹): 1630 (amide, C=O), 3215–3320 (amide CO–NH). ¹H NMR (400 MHz, DMSO-*d*₆) δ (ppm): 4.73 (s, 2H, OCH₂), 6.88–7.78 (m, 13H, Ar–H), 9.64 (s, 1H, NH), 10.11 (s, 1H, NH), 11.80 (s, 1H, NH indole); ¹³C NMR (DMSO-*d*₆) δ : 166.94, 160.61, 156.42, 137.35, 131.48, 131.15, 130.122, 129.68, 129.45, 127.48, 126.42, 126.35, 125.84, 125.53, 124.47, 122.25, 120.45, 116.88, 116.65, 112.91, 104.72, 67.77; LC–MS *m/z* 463 [M+], 466 [M+2]. Anal. Calcd. for C₂₃H₁₈BrN₃O₃ (463): C, 59.50; H, 3.91; N, 9.05. Found: C, 59.44; H, 3.87; N, 9.01%.

1*H*-Indole-2-carboxylic acid {2-[2-(4-chloro-2-methyl-phenoxy)-acetyl-amino]-phenyl}-amide (8i)

Yield: 74%; M.P. 171–173 °C; FT-IR (KBr, ν_{\max} cm⁻¹): 1635 (amide, C=O), 3215–3325 (amide CO–NH). ¹H NMR (400 MHz, DMSO-*d*₆) δ (ppm): 2.54 (s, 3H, CH₃), 4.67 (s, 2H, OCH₂), 6.83–7.77 (m, 12H, Ar–H), 9.63 (s, 1H, NH), 10.22 (s, 1H, NH), 11.84 (s, 1H, NH indole); ¹³C NMR (DMSO-*d*₆) δ : 167.57, 161.63, 156.41, 137.42, 131.55, 131.13, 130.11, 129.65, 129.45, 127.52, 126.46, 126.34, 125.85, 125.51, 124.44, 122.25, 120.48, 116.87, 116.63, 106.90, 103.75, 67.66, 15.11; LC–MS *m/z* 433 [M+], 435 [M+2]. Anal. Calcd. for C₂₄H₂₀ClN₃O₃ (433): C, 66.44; H, 4.65; N, 9.68. Found: C, 60.44; H, 4.59; N, 9.63%.

1*H*-Indole-2-carboxylic acid {2-[2-(2-methoxy-phenoxy)-acetyl-amino]-phenyl}-amide (8j)

Yield: 85%; M.P. 195–197 °C; FT-IR (KBr, ν_{\max} cm⁻¹): 1632 (amide, C=O), 3215–3325 (amide CO–NH). ¹H NMR (400 MHz, DMSO-*d*₆) δ (ppm): 3.88 (s, 3H, OCH₃), 4.62 (s, 2H, OCH₂), 6.85–7.81 (m, 13H, Ar–H), 9.68 (s, 1H, NH), 10.22 (s, 1H, NH), 11.79 (s, 1H, –NH indole); ¹³C NMR (DMSO-*d*₆) δ : 166.94, 160.61, 156.42, 150.35, 131.48, 131.15, 130.122, 129.68, 129.45, 127.48, 126.42, 126.35, 125.84, 125.53, 124.47, 122.25, 120.45, 116.88, 116.65, 113.91, 112.72, 67.77, 56.21; LC–MS *m/z* 416 [M+1]. Anal. Calcd. for C₂₄H₂₁N₃O₄ (415): C, 69.39; H, 5.10; N, 9.54. Found: C, 69.31; H, 5.02; N, 9.50%.

1*H*-Indole-2-carboxylic acid {2-[2-(4-chloro-phenoxy)-acetyl-amino]-phenyl}-amide (8k)

Yield: 89%; M.P. 206–208 °C; FT-IR (KBr, ν_{\max} cm⁻¹): 1635 (amide, C=O), 3212–3320 (amide CO–NH). ¹H NMR (400 MHz, DMSO-*d*₆) δ (ppm): 4.72 (s, 2H, OCH₂), 6.88–7.78 (m, 13H, Ar–H), 9.64 (s, 1H, NH), 10.16 (s, 1H, NH), 11.82 (s, 1H, NH indole); ¹³C NMR (DMSO-*d*₆) δ : 166.95, 160.64, 156.45, 137.42, 131.52, 131.12, 130.11, 129.66, 129.46, 127.50, 126.42, 126.36, 125.82, 125.54, 124.42, 122.26, 120.47, 116.88, 116.62, 112.92, 104.71, 67.77; LC–MS *m/z* 419 [M+], 422 [M+2]. Anal. Calcd. for C₂₄H₂₁N₃O₄ (419): C, 69.40; H, 5.09; N, 10.02. Found: C, 69.33; H, 5.04; N, 10.01%.

1*H*-Indole-2-carboxylic acid [2-(2-phenoxy-acetyl-amino)-phenyl]-amide (8 l)

Yield: 74%; M.P. 177–179 °C; FT-IR (KBr, ν_{\max} cm⁻¹): 1635 (amide, C=O), 3215–3325 (amide CO–NH). ¹H NMR (400 MHz, DMSO-*d*₆) δ (ppm): 4.74 (s, 2H, OCH₂), 6.87–7.75 (m, 14H, Ar–H), 9.66 (s, 1H, NH), 10.21 (s, 1H, NH), 11.80 (s, 1H, NH indole); ¹³C NMR (DMSO-*d*₆) δ : 166.99, 161.05, 156.42, 137.42, 131.50, 131.11, 130.10, 129.67, 129.48, 127.43, 126.40, 126.37, 125.83, 125.53, 124.41, 122.24, 120.48, 117.87, 116.53, 112.90, 111.71, 67.66; LC–MS *m/z* 386 [M+1]. Anal. Calcd. for C₂₃H₁₉N₃O₃ (385): C, 71.67; H, 4.97; N, 10.90. Found: C, 71.61; H, 4.94; N, 10.88%.

1*H*-Indole-2-carboxylic acid {2-[2-(2-bromo-phenoxy)-acetyl-amino]-phenyl}-amide (8 m)

Yield: 77%; M.P. 180–182 °C; FT-IR (KBr, ν_{\max} cm⁻¹): 1630 (amide, C=O), 3210–3330 (amide CO–NH). ¹H NMR (400 MHz, DMSO-*d*₆) δ (ppm): 4.73 (s, 2H, OCH₂), 6.86–7.74 (m, 13H, Ar–H), 9.64 (s, 1H, NH), 10.16 (s, 1H, NH), 11.80 (s, 1H, NH indole); ¹³C NMR (DMSO-*d*₆) δ :

167.06, 162.66, 155.41, 137.43, 131.54, 131.13, 130.10, 129.67, 129.48, 127.50, 126.41, 126.36, 125.83, 125.54, 124.41, 122.25, 120.47, 116.87, 116.63, 112.95, 104.73, 66.89; LC–MS m/z 463 [M+], 465 [M+2]. Anal. Calcd. for $C_{23}H_{18}BrN_3O_3$ (463): C, 59.50; H, 3.91; N, 9.05. Found: C, 59.47; H, 3.88; N, 9.01%.

1*H*-Indole-2-carboxylic acid {2-[2-(2-isopropyl-phenoxy)-acetylamino]-phenyl}-amide (8n)

Yield: 79%; M.P. 174–176 °C; FT-IR (KBr, ν_{\max} cm^{-1}); 1630 (amide, C=O), 3215–3322 (amide CO–NH). ^1H NMR (400 MHz, DMSO- d_6) δ (ppm): 1.20 (d, 6H, CH_3), 3.10 (m, H, CH), 4.75 (s, 2H, OCH_2), 6.85–7.75 (m, 13H, Ar–H), 9.65 (s, 1H, NH), 10.15 (s, 1H, NH), 11.83 (s, 1H, NH indole); ^{13}C NMR (DMSO- d_6) δ : 166.96, 160.65, 156.44, 137.40, 131.51, 131.10, 130.10, 129.67, 129.48, 127.49, 126.43, 126.37, 125.83, 125.55, 124.44, 122.25, 120.48, 116.87, 116.63, 112.90, 111.71, 67.76, 27.50, 23.80; LC–MS m/z 428 [M+1]. Anal. Calcd. for $C_{26}H_{25}N_3O_3$ (427): C, 73.05; H, 5.89; N, 9.83. Found: C, 73.01; H, 5.84; N, 9.80%.

Pharmacology

Materials and methods

Cancer cell lines of human origin, Adenocarcinoma (A549), Breast Carcinoma (MCF-7), Melanoma (A375), mouse cancer cell line, such as Lewis Lung Carcinoma (LLC) and Normal human lung epithelial cells BEAS-2B, HUVEC (human umbilical vein endothelial cell), were obtained from NCCS, Pune, India. Cell culture reagents, DMEM, EGM, antibiotic–anti-mycotic solution, Trypsin–EDTA solution, fetal bovine serum (FBS), poly HEMA (poly hydroxyl methacrylate) from invitrogen (Gibco). Cell cultures were from Eppendorf, Germany. The MTT (3-(4,5-dimethylthiazol-2-yl)-2,5-diphenyl tetrazolium bromide), and BrdU (Bromo-deoxyuridine) cell proliferation assay kit were from Sigma Aldrich. Antibodies against HIF-1 α (hypoxia-inducible factor-1 alpha), VEGF (vascular endothelial growth factor), MMP-2 (Matrix Metallo Proteinase-2), MMP-9 (Matrix Metallo Proteinase-9), were procured from Santa Cruz Biotechnology Inc, USA. The immunostaining kit was from Leica Biosystems, Germany. Eggs for CAM were procured from Indian Veterinary Research Institute (IVRI) Bengaluru, Karnataka, India. All other chemicals including solvents used were purchased from Hi-Media, Mumbai, India. All bright field and fluorescence images were documented in EVOS FL cell imaging, Thermo Scientific, USA. Quantification of angiogenesis was carried out by ImageJ software (NIH, Bethesda, MD, USA).

Cell culture and in vitro anti-proliferative studies

Listed cell lines A549, MCF-7, A375, LLC and BEAS-2B were grown in DMEM with 10% FBS, enriched in antibiotic–anti-mycotic solution (100 $\mu\text{g}/\text{ml}$), sodium carbonate (0.37%) and incubated at 37 °C in 5% CO_2 , with \geq 98% humidity. The anti-proliferative efficiency of **IPA (8a–n)** (0, 2, 5, 10, 25, and 50 μM in DMSO) was evaluated through MTT release assay. The average IC_{50} values were calculated as described earlier [16]. The DMSO and 5-fluorouracil were used as a vehicle and positive control, respectively.

The BrdU cell proliferation assay was performed as per manufacturer protocol. In brief, cultured confluence cells were treated with or without **IPA (8k)** (0, 3, and 5 μM) for 48 h, followed by 10 μM BrdU incorporation. Cells were washed, fixed, permeabilized, and treated with anti-BrdU primary antibody. Cells were counterstained with 4',6-diamidino-2-phenylindole (DAPI) and visualized under the microscope, documented.

Chorioallantoic membrane (CAM) assay

The in vivo anti-angiogenic effect of **IPA (8k)** was performed as reported earlier [17]. In brief, 6 days of pre-incubated eggs (each groups containing $n = 6$ eggs) were surface-sterilized, made window, and induced with recombinant VEGF-10 ng/CAM (rVEGF $_{165}$). The growing CAM was treated with **IPA (8k)** (0, 3, 5 $\mu\text{g}/\text{CAM}$). After 48 h, variation in the blood vessel formation was visually documented and quantified.

Rat corneal micro-pocket assay

To evaluate the angioinhibitory effect of **IPA (8k)**, the rat corneal micro-pocket assay was performed as reported earlier [18]. In short, the sprouting angiogenesis was induced in rat cornea by applying rVEGF $_{165}$ (10 ng/pellet) and treated with **IPA (8k)** (0, 3, 5 $\mu\text{g}/\text{pellet}$) using formulated poly HEMA. Corneal angiogenesis and re-modulation were measured in histopathological studies (H and E). The MVD (Micro Vessel Density) number was quantified and graphically represented.

Hypoxic conditions, in vitro treatment and lysate preparations

To examine the **IPA (8k)** efficacy on the anti-proliferative mechanism, A549 cells were treated at different concentrations (0, 3 and 5 μM) under normoxic, pseudohypoxic and hypoxic environments. The pseudohypoxic microenvironment was created by treating the cells with CoCl_2 (100 μM) for 48 h before **IPA (8k)** treatment. For hypoxia, cells were grown in a hypoxia chamber with a gas supply containing

1% O₂, 5% CO₂ and 94% N₂, and exposed with **IPA (8k)**. The cells were harvested and whole cell lysate was used for further Immunoblot (IB) studies. Cell-free conditioned medium was used for gelatin zymogram and ELISA studies [18, 19].

HUVEC cell migration and tube formation assay

The confluence monolayer HUVECs grown in a 96-well plate and 1 mm size wounds were made by scratching with a microtip and exposed with rVEGF₁₆₅ (30 ng/ml) and **IPA (8k)** (0, 3, 5 μ M) for 48 h. The migrated cells locations were photographed at identical locations and analyzed by comparing final gap width to initial gap width. ECM gel was polymerized for 30 min at 37 °C for coating 96-well plate. HUVECs suspended in EGM medium was added to each well coated with ECM gel and treated with or without rVEGF₁₆₅ and **IPA (8k)** (0, 3, 5 μ M) for 24 h. Inhibition in the formation tube and its lengths was documented [18].

Gelatin zymography

Gelatin zymography is one of the most suitable assays to quantify the secreted MMP-2 and MMP-9 concentration [20]. In brief, conditioned media from the cultured A549 cells were treated with or without **IPA (8k)** (0, 3, and 5 μ M) for 48 h and resolved in 8% SDS-PAGE gel containing 0.1% (w/v) dissolved gelatin and the zymogram was developed. The decrease of gelatin lysis zone was documented using Bio-rad Gel Documentation™ XR + Imaging System.

Animal models and ethics

Healthy BALB/c mice weighing (27–30 g) were used in *in vivo* studies [21]. All the experiments performed on animals were maintained as per CPCSEA guidelines with the permission of the Institutional Animal Ethics Committee (Ref No. KSHEMA/IAEC/01/2018).

Animal tumor models and treatment

Dalton's lymphoma (DL) solid tumor was developed by adopting the earlier reported procedure [22]. In brief, DLA (5×10^6 cells) was injected into the thigh region of the mice subcutaneously (*sc*) to develop a solid tumor (DLS). After the onset of tumor development to 100 mm³ in size, mice were administered with **IPA (8k)** (0, 30 and 50 mg/kg) *bw* ($n=6$ each) for six doses (*ip*) for every alternate day. At the end of the 35th day from tumor implantation, the tumor tissues were dissected and photographed. The tissue lysate from treated and untreated group mice were prepared for IB and gelatin zymography analysis. Tumour tissues were further processed immunohistochemistry (IHC) analysis.

Serum collected was used for measurement of VEGF, alkaline phosphatase (ALP), creatinine, urea, RBC and WBC from each group. Survivability of the mice bearing DLS tumor-treated mice ($n=10$ each) was monitored separately.

Immunohistochemistry (IHC)

The histopathological assessments of MVD and IHC analysis were performed for HIF-1 α using dissected DLS tumor tissue [23]. The IHCs were independently evaluated by two pathologists and documented.

VEGF-ELISA

The *in vitro* and *in vivo* secretions of VEGF levels were quantified using anti-VEGF antibody through ELISA [24]. In brief, 100 μ l of conditioned media (*in vitro*) and serum (*in vivo*) was coated in coating buffer at 4 °C overnight and incubated with anti-VEGF-A antibody, followed by re-incubation with ALP conjugated secondary antibody. Quantification of secreted VEGF-A was measured at 405 nm.

Immunoblots

Immunoblot (IB) analysis was performed for HIF-1 α , p53, MMP-2, MMP-9, and β -actin proteins as mentioned earlier [25]. The protein lysate prepared from **IPA (8k)**-treated and -untreated conditions was resolved on SDS-PAGE and transferred to nitrocellulose membrane. The blots were probed with appropriate antibodies and images were densitometrically quantified.

Statistical analysis

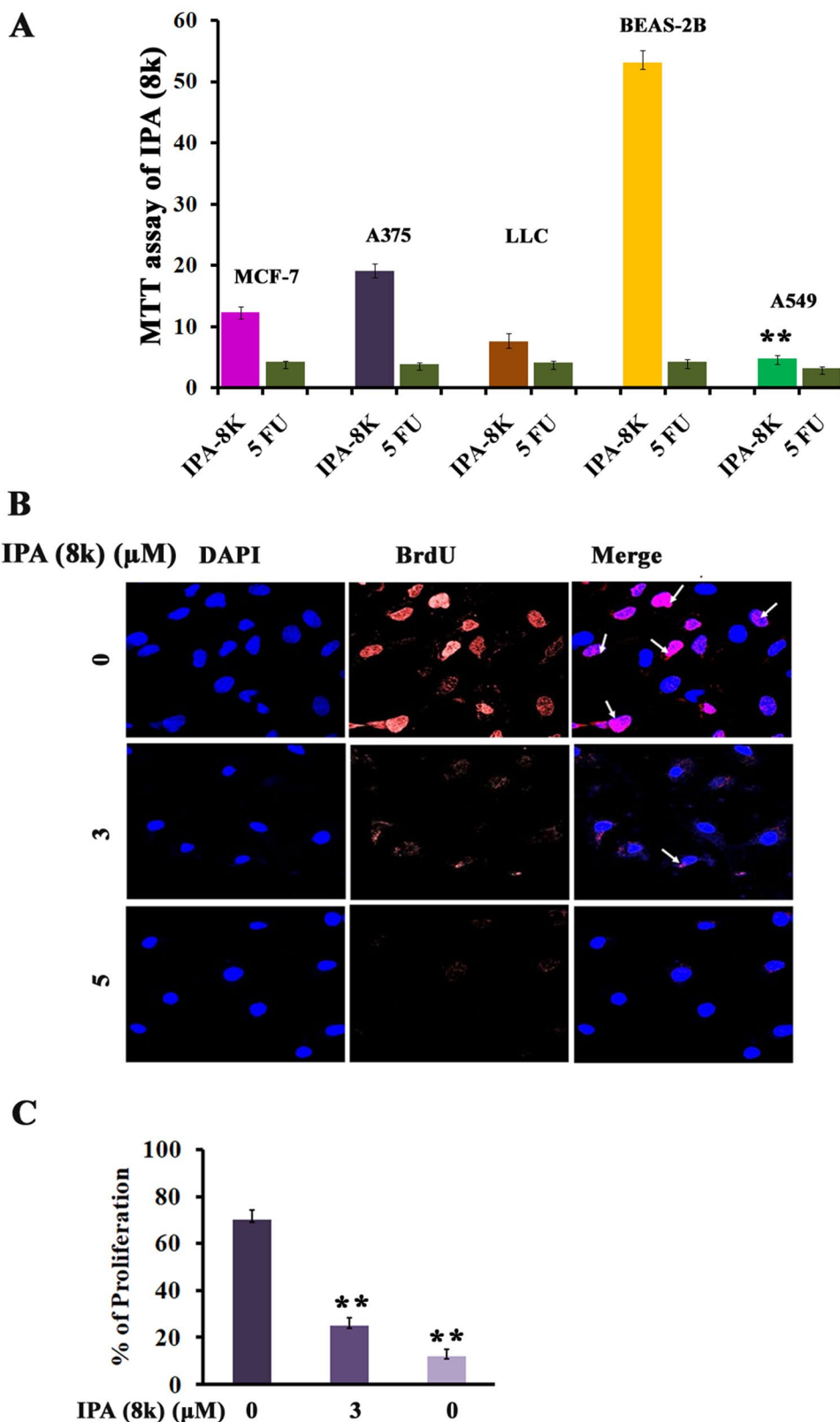
All *in vitro* experiments were repeated three times independently and statistically analysed through one-way ANOVA followed by Brown–Forsythe test. The results are expressed as mean \pm standard deviation (SD). All *in vivo* experiments involved six variables per group and were repeated three times independently. Data were analysed using one-way ANOVA followed by Brown–Forsythe test. The results are expressed as mean \pm standard deviation (SD). Statistical significance was set at * $p < 0.05$ to **** $p < 0.0001$. All data analyses were performed using Graph pad prism version 8.0.

Results and discussion

Chemistry

Scheme 1 showed the synthetic methods for the new **IPA (8a–n)** analogs. The preparations of the title compounds **IPA (8a–n)** were started with commercially available substituted

Fig. 1 IPA (**8k**) shows induces cytotoxicity against the A549 cells: the various cancer cell lines were treated with varied concentrations of IPA (**8a–n**) for 48 h and cell proliferation rate was measured by MTT assay. **a** IPA (**8k**) showing the IC_{50} value of $5 \mu M$ against the A549 cell with potent cytotoxicity activity more or less similar to 5-Fu. **b, c** Antiproliferative efficacy of IPA (**8k**) in BrdU proliferation assay with proliferation inhibition graph. Graphs were plotted by taking mean ($n = 3$) \pm SD. Statistical analysis was performed using one-way ANOVA followed by Brown-Forsythe test and statistical significance was set at $*p < 0.05$ to $****p < 0.0001$



phenols (**1a–h**) which easily refluxed with ethyl chloroacetate (**2**) in the presence of anhydrous potassium carbonate and acetone as a suitable solvent. The reaction mixture was

monitored using TLC until the completion of the reaction to achieve corresponding phenoxy esters (**3a–h**). In the second step, hydrolysis of the compounds (**3a–g**) was carried out

Table 1 MTT IC₅₀ values of compounds **IPA (8a–n)**

Cell lines	IPA (8K)	IPA (8C)	IPA (8G)	IPA (8I)	IPA (8H)	IPA (8A)	IPA (8E)	IPA (8F)	IPA (8B)	IPA (8M)	IPA (8J)	IPA (8N)	IPA (8L)	IPA (8D)	5-FU
A549	5.0 ±0.59	46.21 ±1.83	48.83 ±1.85	52.6 ±1.85	51.25 ±2.5	32.35 ±1.2	45.6 ±1.75	53.21 ±1.5	62.35 ±1.25	64.9± 0.8	62.5± 2.3	48.5 ±1.8	54.5± 1.6	71.23 ±1.97	3.9 ±0.59
MCF-7	14.2 ±0.26	42.23 ±2.8	55.29 ±2.39	56.2 ±1.67	59.52 ±2.2	45.56 ±2.8	44.6 ±2.25	55.23 ±2.2	55.56 ±2.2	66.7± 0.9	64.2± 2.1	55.8± 2.5	62.1± 1.9	72.25 ±1.93	4.2 ±0.26
A375	16.2 ±0.98	42.52 ±1.25	56.59 ±2.25	54.9 ±1.85	53.15 ±2.5	46.16 ±1.1	46.7 ±1.04	58.56 ±1.8	66.16 ±1.8	64.6± 0.9	68.8± 1.8	64.6± 1.9	68.6± 1.5	73.25 ±2.87	3.8 ±0.98
LLC	7.5 ±0.59	38.25 ±1.95	45.56 ±2.29	52.23 ±0.9	49 ±1.85	51.29 ±1.63	53.59 ±2.37	59.6 ±1.78	61.29 ±0.58	65.62 ±1.98	65.21 ±1.59	65.95 ±1.69	71.2 ±1.68	74.5 ±1.5	4.2 ±0.51
BEA S-2B	49.3 ±1.38	56.29 ±1.1	61.41 ±2.02	61.2 ±1.86	58.33 ±2.3	52.31 ±1.6	49.2 ±2.98	58.59 ±1.2	92.12 ±2.65	83.7 ±1.5	73.2 ±1.3	92.5 ±2.5	79.8 ±1.2	75.78 ±2.85	5.0±1 .38

using an ethanolic solution of sodium hydroxide to afford the appropriate phenoxy acetic acid analogs (**4a–h**). Moreover, the coupled product phenoxy acetamide derivatives (**6a–h**) were synthesized by condensation of compounds (**4a–h**) with *O*-phenylenediamine (**5**), at a low temperature around 5 °C using DCM as a suitable solvent and 2,6 lutidine and *O*-(benzotriazol-1-yl)-*N,N,N',N'*-tetramethyluroniumtetrafluoroborate (TBTU) used as a coupling agent. Finally, the title compounds **IPA (8a–n)** were synthesized by the treatment of the compounds (**4a–h**) with (**6a–h**) using the above condition to affirm the expected title product **IPA (8a–n)** with the yield in the range of 74–89%.

Furthermore, all the synthesized compounds have been proved by FT-IR, ¹H NMR, ¹³C NMR and mass spectra characterization. For instance, among the synthesized series **IPA (8a–n)**, the compound (**8d**) was taken as an example. The FT-IR spectrum of compound **IPA (8d)** proved by the appearance of two CO–NH stretching bands in the range 3210–3320 cm⁻¹ and disappearance of both carboxylic and amino groups stretching bands of compounds (**7a**) and (**6d**), respectively (Supplementary S1). Interestingly, the ¹H NMR spectrum of compound **IPA (8d)** showed the disappearance of the protons of the carboxyl group as well as the amino group of the compounds (**7a**) and (**6d**), respectively, and also the appearance of new protons for two NH groups at δ 9.57 ppm and 9.68 ppm (Supplementary S2). The compound **IPA (8d)** was also supported by inspecting the ¹³C NMR and mass spectrum with a significant M + 1 peak at *m/z* 400 (Supplementary S3 and 4).

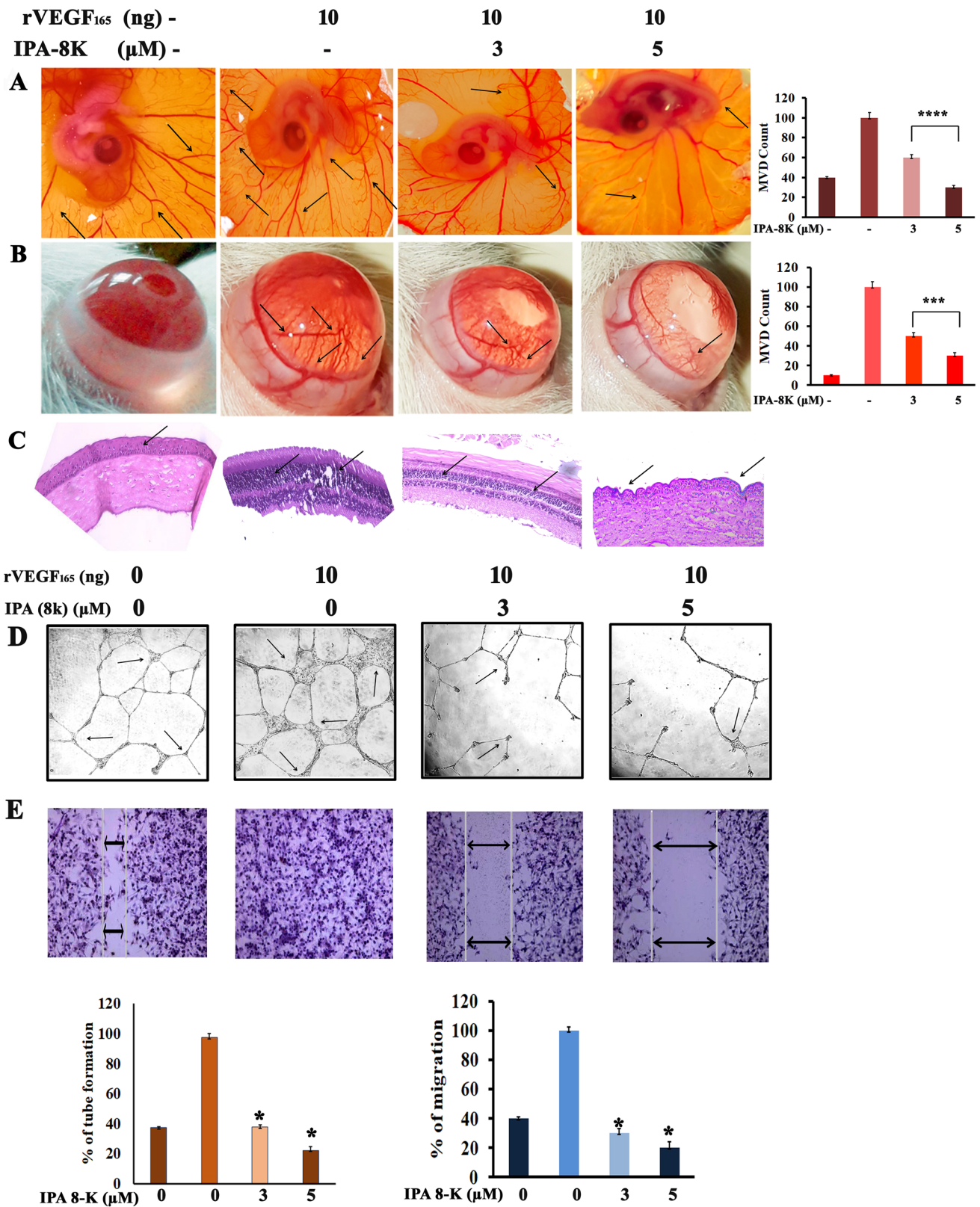
Biology

IPA (8k) as a lead compound and SAR

The current investigation mainly focused on identifying and developing a new active anti-proliferative/cytotoxic molecule inhibitor for tumor angiogenesis with specific

target. Based on the investigation results, one of the major drawbacks in establishing such cancer therapy is failing to reach the translational side either due to their non-specificity or adverse side effects [26]. In this view, designing a molecule that specifically counteracts these problems is the foremost essential requirement. With this notion, we have synthesized **IPA (8a–n)** analogs which are known to be pharmacologically active molecules against various pathological conditions such as solid tumors [27]. The development of an active drug always relies on screening against various cancer cell lines with a different origin for better evaluation [28]. Therefore, newly synthesized **IPA (8a–n)** analogs were initially screened for their in vitro cytotoxic and anti-proliferative activity against cell lines, such as A549, MCF-7, A375, LLC and normal BEAS-2B. Among **IPA (8a–n)** analogs, **IPA (8k)** showed promising anti-proliferative potency with an IC₅₀ value of 5 μ M specifically against A549 cells as verified by MTT assay (Fig. 1a) without affecting normal cell counterpart. Our preliminary investigation infers that the **IPA (8k)** with electron-withdrawing chloro group at para position of the

Fig. 2 **IPA (8k)** attenuates the neovessel formation in non-tumoral ► angiogenic models: The growing CAM and rat cornea was stimulated for angiogenesis with rVEGF₁₆₅ and treated with or without **IPA (8k)** for 48 h. **a** The in vivo CAM results symbolize the inhibition of neovessel formation by declining the MVD density with graph. **b** Modulation in the sprouting of neovessel formation in rat cornea with decreased MVD with respective graph. **c** H&E staining shows the effect of the compound **IPA (8k)** in the normalization of the cornea with decrease in the MVD. Antimigratory and tube formation effect of endothelial cells were measure in HUVEC's cells treated with or without **IPA (8k)** for 48 h. **d** Regression of capillary tube formation ability of the HUVECs. **e** Inhibition in the migration of the endothelial cells to heal the wound with quantified representation. Graphs were plotted by taking mean ($n=6$ for Fig. 2a, b and $n=3$ for Fig. 2d, e) \pm SD. Statistical analysis was performed using one-way ANOVA followed by Brown-Forsythe test and statistical significance was set at * $p < 0.05$ to **** $p < 0.0001$



phenoxy ring has potent cytotoxicity against the A549 cells. The results are on par with the standard drug 5-fluorouracil (Table 1). Analyzing the activity data revealed

that other IPA (8c, 8g, 8i, 8h, 8a, 8e and 8f) analogs with electron-withdrawing halo groups at para position showed moderate anti-proliferative potency in decreasing order.

While the other compounds with different substituents have not shown significant activity (Table 1). The anti-proliferative effect of **IPA (8k)** was further validated and confirmed by BrdU cell proliferation assay with a significant reduction in the rate of proliferation (Fig. 1b, c).

IPA (8k) induces angioinhibitor

The process of angiogenesis in neoplasia involves several basic steps, such as hypoxia, ischemia, blood vessel damage and elevated expression of proangiogenic growth factors and resulting in the formation of the new blood vessels [29]. The VEGF being one such predominant growth factor plays an important role in the stimulation of angiogenesis and used in reliable non-tumor angiogenesis assay models, such as CAM and rat corneal micro-pocket assay, which are well authenticated for its target-specific action towards neovascularization [25, 30]. The mechanism underlying the anti-proliferative efficacy of **IPA (8k)** was evaluated in a non-tumorigenic *in vivo* CAM model to detect the inhibition of angiogenesis. The results interpreted that, **IPA (8k)** drastically reduced the rVEGF₁₆₅-induced MVD in a concentration-dependent manner up to 40 and 60%, respectively, when compared with rVEGF₁₆₅-induced control CAM (Fig. 2a). The anti-angiogenic efficacy of **IPA (8k)** was additionally evaluated by the corneal neovascularization inhibition potency by an enthusing cornea with rVEGF₁₆₅. Results inferred that sprouting concentration of the neoangiogenesis through the cornea was blocked up to 50 and 70% when compared to the control corneal neovascularization concentration-dependent manner. Also, **IPA (8k)** was able to improve the remodulation of corneal neoangiogenesis gesture (Fig. 2b, c).

Further, HUVECs capillary tube formation assay results postulated that **IPA (8k)** evidently stops the human functional endothelial cell migration adjacent linkage and capillary tube formation efficiency by exhibiting the irregular cellular morphology up to 65 and 80% in their respective treatment manner. Tube length and branch number were also drastically reduced by **IPA (8k)** (Fig. 2d). Supportive to this, the effect of **IPA (8k)** on the invasive and migration property of A549 cells was evaluated. The relative migration capability of A549 cells to heal the wound distance was significantly shorter in **IPA (8k)** treated cells with 25.65% and 17.32% in 3 and 5 μ M concentrations, respectively (Fig. 2E).

IPA (8k) inhibits HIF-1 α and its downstream signaling

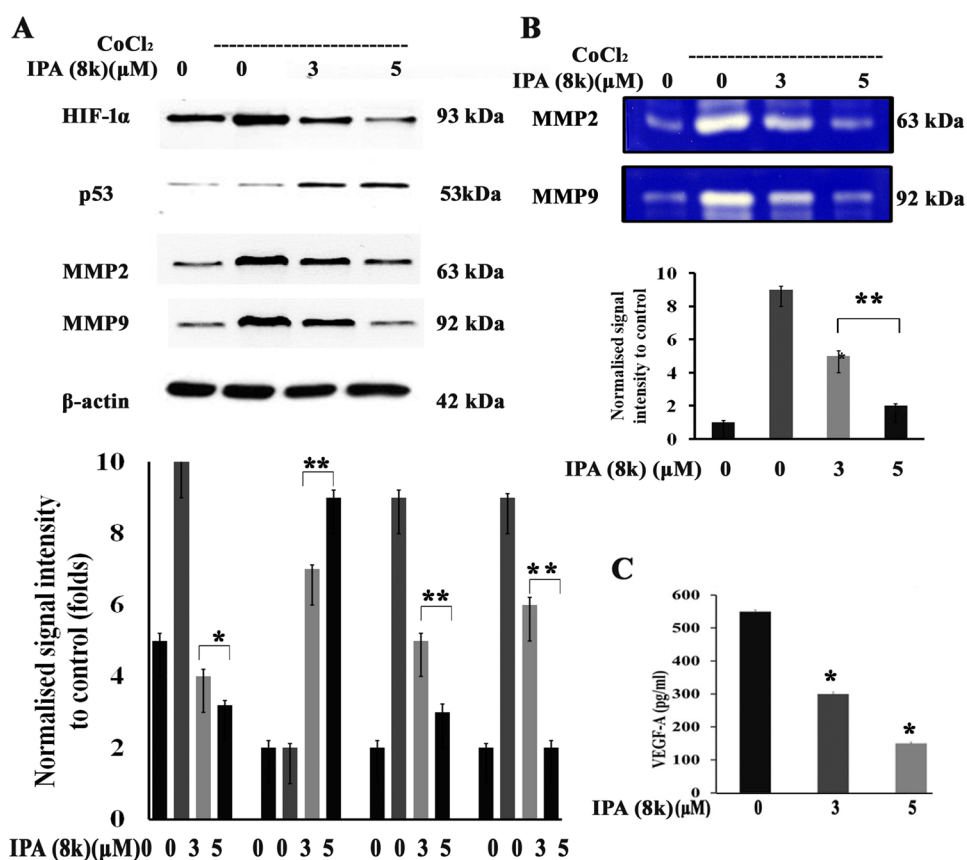
The HIF-1 α is key transcription factor expressed under a solid tumor microenvironment. The associations between HIF-1 α with angiogenesis for tumor growth promotion have been well established in many solid tumor studies. The HIF-1 α takes part in every step of angiogenesis by interacting with several cellular signaling molecules, thereby

participating in the tumor progression. This cross-interaction of HIF-1 α and proangiogenic factors is the base for the capillary formation under hypoxic conditions. Initiation of the angiogenesis under hypoxic conditions primarily activated by HIF-1 α and mainly dependent on VEGF followed by the MMPs [31]. All these create the hyper-recognition towards HIF-1 α and its downstream pathway as an attractive target in cancer research. Even though several small molecules with different chemotypes and intense biological potency were reported to be promising HIF-1 α inhibitors, but none of the available drugs were clinically approved [3]. In this connection, efforts in this direction are necessary to establish, targeted therapy towards the HIF-1 α inhibition. In the current investigation, **IPA (8k)** efficacy in inhibition of the HIF-1 α was evaluated. The hypoxic microenvironment is created by treating the cells with CoCl₂ before **IPA (8k)** treatment in a concentration-dependent manner. The results imply that **IPA (8k)** effectively inhibits the HIF-1 α expression which creates an obstacle to the tumor cells to overcome by hypoxic condition (Fig. 3a). The HIF-1 α -dependent expression of the MMP-2 and MMP-9 in the treated cell was reduced significantly as verified in both IB and zymogram analysis (Fig. 3b). Down the line, anti-tumoral gene p53 was elevated in concentration-dependent manner (Fig. 3a). One of the major angiogenic initiating factors VEGF-A expression level has direct reflection with the aggressive tumor angiogenesis [31]. The treatment of **IPA (8k)** drastically reduces the VEGF-A secretion and thereby attenuates the angiogenesis promotion (Fig. 3c).

IPA (8k) suppresses solid tumor

Tumor hypoxia is an important hurdle to the effective treatment of cancer. Hypoxia exists in most solid tumors due to insufficient oxygen supply of the abnormal vasculature formation which results in the high demands of oxygen by rapidly proliferating cancer cells. The capability of the drug efficacy was always confirmed by the reflecting results as shown in an *in vitro* condition, in the development of the novel potent pharmacophores. DLA Solid (DLS) tumor model is the most widely used vital model for the investigation of drug efficacy, within the natural tumor hypoxic condition as a hypoxia inhibitor. Based on the evidential results from *in vitro* data, the anti-tumoral effect of the **IPA (8k)** was reconfirmed in an *in vivo* DLS tumor model system. The drug dosage concentrations (0, 30 and 50 mg/kg b.w) for the treatment of the compound **IPA (8k)** for an *in vivo* study were determined by LD₅₀ assay, by simultaneously assessing the possible impact on hematological and hepatological side effects. The results referred that **IPA (8k)** does not induce any significant toxicological effect in the murine model system (Supplementary S20).

Fig. 3 IPA (8k) targets HIF-1 α gene expression and modulates its downstream signaling. Whole cell lysate and conditioned media from the IPA (8k) treated A549 (0, 3, 5 μ M) cells were subjected to IB and gelatin zymography analysis. **a** Suppression of HIF-1 α and its downstream MMP-2 and MMP-9 gene expression with elevation in the p53 gene expression and their respective densitometry graph. **b** Decreased gelatinase activity of MMP-2 and MMP-9. **c** Decrease in the production of the VEGF-A in the conditioned media. Graphs were plotted by taking mean ($n=3$) \pm SD. Statistical analysis was performed using one-way ANOVA followed by Brown-Forsythe test and statistical significance was set at * $p < 0.05$ to *** $p < 0.0001$



The treatment of IPA (8k) on the DLS tumor model attenuates the tumor progression in a dose-dependent manner which is reflected in the enhanced survival period with noticeable and improved physiology (Fig. 4 A, B, C and D). The inhibitory effect of solid tumor progression is due to the inhibition of MVD as verified by H and E staining. The MVD count was significantly down in IPA (8k) treated cells in a concentration-dependent manner (Fig. 4e, f). Since MVD strongly relies on HIF-1 α -dependent VEGF levels, we verified the expression of HIF-1 α in both IHC and IB analysis (Fig. 4g–i). Results reconfirmed the in vitro data. Eventually, modulation in the expression levels of its relevant genes MMP-2, MMP-9, P53 and VEGF as verified by zymogram, IB and ELISA (Fig. 4j, k). Overall, the IPA (8k) could be developed into an inhibitor of HIF-1 α with minimal cytotoxicity and provides the mechanism-based evidence for the possible drug development for cancer therapy.

Statistical results

Each experiment was statistically analyzed and results are expressed in terms of **f**, **df**, and **p** values and tabulated (Supplementary Table 1).

Conclusion

One of the most terrifying health issues is cancer, which has driven chemists and other concerned parties to struggle for the development of efficient medicines with new strategies. Clinical development of anti-angiogenic molecules for cancer therapy was a success and translated into approved treatment in many cancers. Tumor hypoxia acts as a prevalent and major barrier to effective cancer treatment. A diversity of different methods has been employed to reverse tumor hypoxic environment and to date, there are no Food and Drug Administration (FDA) approved treatments to reverse tumor hypoxia. As a continued effort, in the present investigation, IPA (8k) with chloro group at the para position can induce cell-specific cytotoxic effects and can effectively inhibit neovascularization in both in vitro and in vivo by inhibiting the HIF-1 α , a master protein that plays a critical role in the tumor cell survival. Overall, our results postulate IPA (8k) has the potential to inhibit the solid tumor progression by blocking one of the major hallmarks of cancer by specifically targeting HIF-1 α and provides scope for anti-angiogenic-based therapies.

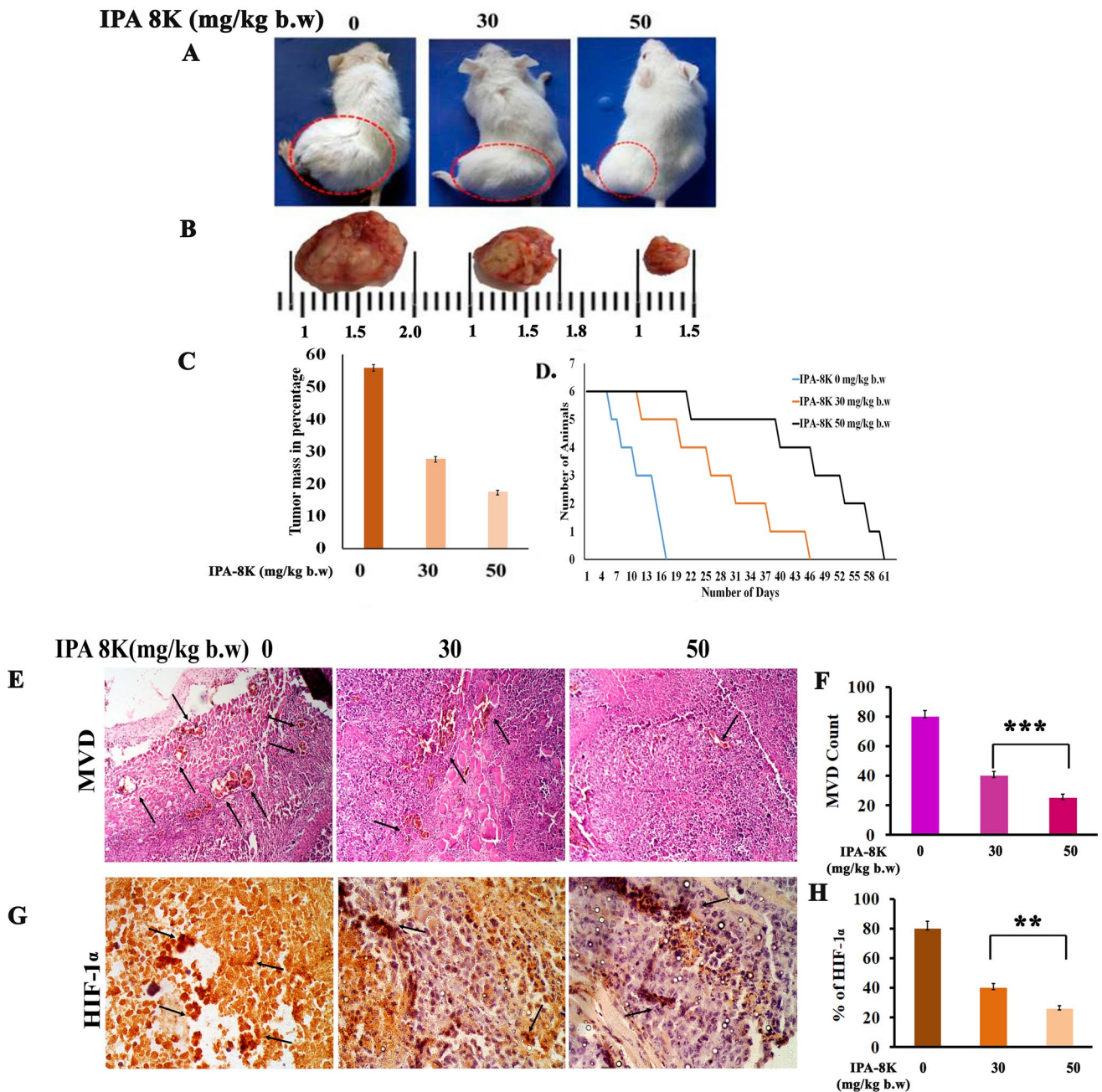


Fig. 4 IPA (8k) inhibits in vivo DL Solid tumor (DLS) with HIF-1 α inhibitory mechanism. DLA cells (5×10^6 cells/thigh *sc*) were injected into the thigh of to induce solid tumor. After onset of the tumor, mice were grouped and administered with **IPA (8k)** (0, 30 and 50 mg/kg b.w (*ip*) for 6 doses on every two alternative days. At the end of 35th day, tumor parameters were examined and cell lysate was subjected to the gene expression analysis. **a, b** Morphology of solid tumor bearing mice with tumor section. **c** Percentage of mass of tumor inhibition. **d** Kaplan Meyer graph for extended mice survivality. **e, f** H&E staining for MVD and its quantification. **g, h** IHC

studies shows the expression levels of the HIF-1 α and its relative expression level **i**. Suppression of HIF-1 α expression and downstream MMP-2 and MMP-9 genes expression with elevation in the anti-tumor p53 gene expression with their respective densitometry graph. **j** Decreased gelatinase activity of MMP-2 and MMP-9. **k** Decrease in the production of the VEGF-A in the serum. Graphs were plotted by taking mean ($n=6$) \pm SD. Statistical analysis was performed using one-way ANOVA followed by Brown-Forsythe test and statistical significance was set at $*p < 0.05$ to $****p < 0.0001$

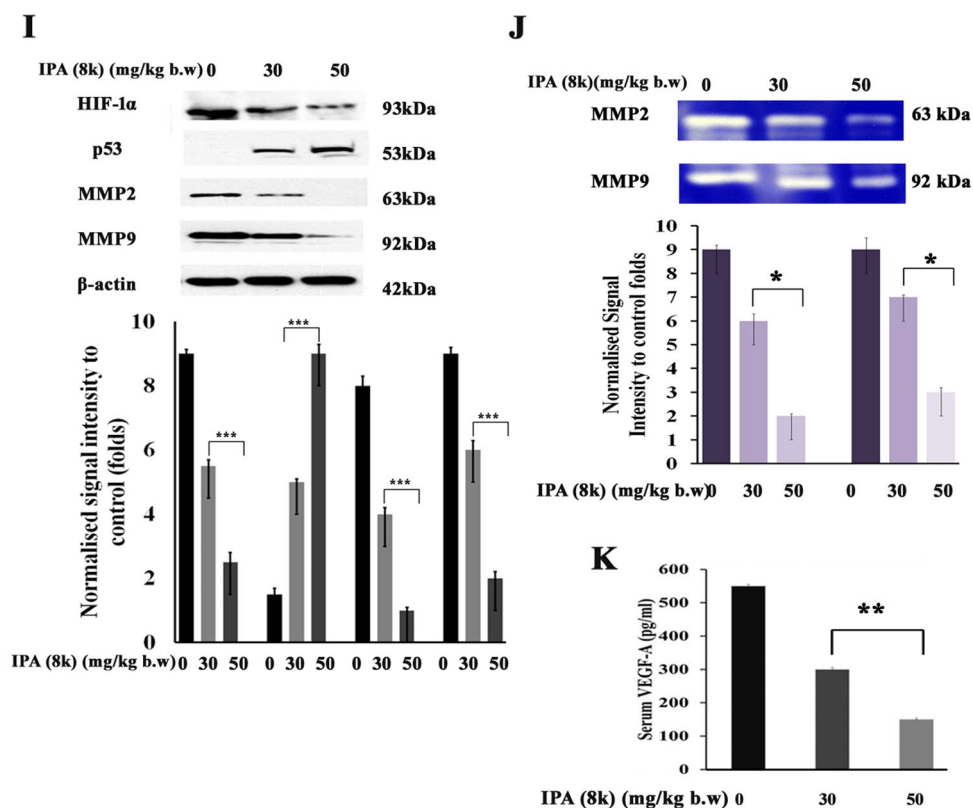


Fig. 4 (continued)

Supplementary Information The online version contains supplementary material available at <https://doi.org/10.1007/s43440-021-00266-8>.

Acknowledgements Fares Hezam Al-Ostoot is thankful to the government of Yemen and Al-Baydha University, Yemen, for providing financial assistance under the teacher's fellowship and also thankful to the University of Mysore, Mysore, India. Ankith Sherapur thanks the Lady Tata Memorial Trust for JRS (2020–2021) and B.T. Prabhakar gratefully acknowledges the grant support by VGST (VGST/P-2/CISEE/GRD-231/2013-14) and SERB [EMR/2017/00088/dated 3/01/2019]. Shaikath Ara Khanum thankfully acknowledges the financial support provided by VGST, Bangalore, under CISEE Program [Project sanction order: No. VGST/CISEE/282/2012-13].

Author contributions FHA and AS performed all the experiments, VV and HKV assisted in experiments, GB supported through statistical analysis, SAK and PBT designed the experiments, wrote the manuscript and monitored the entire investigation.

Declarations

Conflict of interest The authors declare that there are no conflicts of interest.

References

- Zimna A, Kurpisz M. Hypoxia-inducible factor-1 in physiological and pathophysiological angiogenesis: applications and therapies. *BioMed Res Int.* 2015;2015:549412.
- Semenza GL. Hypoxia-inducible factor 1 and cardiovascular disease. *Annu Rev Physiol.* 2014;76:39–65.
- Ma Z, Xiang X, Li S, Xie P, Gong Q, Goh BC, et al. Targeting hypoxia-inducible factor-1, for cancer treatment: recent advances in developing small-molecule inhibitors from natural compounds. *Semin Cancer Biol.* 2020. <https://doi.org/10.1016/j.semcancer.2020.09.011>.
- Fuse S, Suzuki K, Kuchimaru T, Kadonosono T, Ueda H, Sato S, et al. Design, synthesis, and evaluation of indeno [2, 1-c] pyrazolones for use as inhibitors against hypoxia-inducible factor (HIF)-1 transcriptional activity. *Bioorganic Med Chem.* 2020;28:115207.
- Jin X, Dai L, Ma Y, Wang J, Liu Z. Implications of HIF-1 in the tumorigenesis and progression of pancreatic cancer. *Cancer Cell Int.* 2020;20:1–11.
- Gurupadaswamy HD, Thirusangu P, Avin BV, Vigneshwaran V, Kumar MP, Abhishek TS, et al. DAO-9 (2, 5-di (4-aryloxyloxy-methyl)-1, 3, 4-oxadiazole) exhibits p53 induced apoptosis through caspase-3 mediated endonuclease activity in murine carcinoma. *Biomed Pharmacother.* 2014;68:791–7.

7. Shimazaki Y, Yajima T, Takani M, Yamauchi O. Metal complexes involving indole rings: structures and effects of metal–indole interactions. *Coord Chem Rev.* 2009;253:479–92.
8. Demurtas M, Baldisserotto A, Lampronti I, Moi D, Balboni G, Pacifico S, et al. Indole derivatives as multifunctional drugs: synthesis and evaluation of antioxidant, photoprotective and antiproliferative activity of indolehydrazones. *Bioorganic Chem.* 2019;85:568–76.
9. Lakshmi NV, Thirumurugan P, Noorulla KM, Perumal PT. InCl₃ mediated one-pot multicomponent synthesis, anti-microbial, antioxidant and anticancer evaluation of 3-pyranyl indole derivatives. *Bioorganic Med Chem Lett.* 2010;20:5054–61.
10. Merino I, Monge A, Font M, de Irujo JJ, Alberdi E, Santiago E, et al. Synthesis and anti-HIV-1 activities of new pyrimido [5, 4-b] indoles. *IFarmacology.* 1999;54:255–64.
11. Brew CT, Aronchik I, Hsu JC, Sheen JH, Dickson RB, Bjeldanes LF, et al. Indole-3-carbinol activates the ATM signaling pathway independent of DNA damage to stabilize p53 and induce G1 arrest of human mammary epithelial cells. *Int J Cancer.* 2006;118:857–68.
12. Meng Q, Qi M, Chen DZ, Yuan R, Goldberg ID, Rosen E, et al. Suppression of breast cancer invasion and migration by indole-3-carbinol: associated with up-regulation of BRCA1 and E-cadherin/catenin complexes. *J Mol Med.* 2000;78:155–65.
13. Al-Ostoot FH, Geetha DV, Mohammed YH, Akhileshwari P, Sridhar MA, Khanum SA. Design-based synthesis, molecular docking analysis of an anti-inflammatory drug, and geometrical optimization and interaction energy studies of an indole acetamide derivative. *J Mol Struct.* 2020;1202:127244.
14. Al-Ostoot FH, Grisha S, Mohammed YH, Vivek HK, Khanum SA. Molecular docking and synthesis of caffeic acid analogous and its anti-inflammatory, analgesic and ulcerogenic studies. *Bioorganic Med Chem Lett.* 2021;33:127743.
15. Khamees HA, Mohammed YH, Swamynayaka A, Al-Ostoot FH, Sert Y, Alghamdi S, et al. Molecular structure, DFT, vibrational spectra with fluorescence effect, hirshfeld surface, docking simulation and antioxidant activity of thiazole derivative. *ChemistrySelect.* 2019;4:4544–58.
16. Ranganatha VL, Avin BV, Thirusangu P, Prashanth T, Prabhakar BT, Khanum SA. Synthesis, angiopreventive activity, and in vivo tumor inhibition of novel benzophenone–benzimidazole analogs. *Life Sci.* 2013;93:904–11.
17. Vijay Avin BR, Thirusangu P, Ranganatha VL, Firdouse A, Prabhakar BT, Khanum SA. Synthesis and tumor inhibitory activity of novel coumarin analogs targeting angiogenesis and apoptosis. *Eur J Med Chem.* 2014;75:211–21.
18. Thirusangu P, Vigneshwaran V, Prashanth T, Avin BV, Malojirao VH, Rakesh H, et al. BP-1T, an antiangiogenic benzophenone-thiazole pharmacophore, counteracts HIF-1 signalling through p53/MDM2-mediated HIF-1 α proteasomal degradation. *Angiogenesis.* 2017;20:55–71.
19. Vigneshwaran V, Thirusangu P, Vijay Avin BR, Krishna V, Pramod SN, Prabhakar BT. Immunomodulatory glc/man-directed Dolichos lablab lectin (DLL) evokes anti-tumour response in vivo by counteracting angiogenic gene expressions. *Clin Exp Immunol.* 2017;189:21–35.
20. Avin BV, Prabhu T, Ramesh CK, Vigneshwaran V, Riaz M, Jayashree K, et al. New role of lupeol in reticence of angiogenesis, the cellular parameter of neoplastic progression in tumorigenesis models through altered gene expression. *Biochem Biophys Res Commun.* 2014;448:139–44.
21. Zabiulla Z, Malojirao VH, Mohammed YH, Thirusangu P, Prabhakar BT, Khanum SA. Synthesis, molecular docking, and apoptogenic efficacy of novel *N*-heterocycle analogs to target B-cell lymphoma 2/X-linked inhibitors of apoptosis proteins to regress melanoma. *Med Chem Res.* 2019;28:1132–60.
22. Vigneshwaran V, Thirusangu P, Madhusudana S, Krishna V, Pramod SN, Prabhakar BT. The latex sap of the ‘Old World Plant’ *Lagenaria siceraria* with potent lectin activity mitigates neoplastic malignancy targeting neovasculature and cell death. *Int Immunopharmacol.* 2016;39:158–71.
23. Thirusangu P, Vigneshwaran V, Ranganatha VL, Avin BV, Khanum SA, Mahmood R, et al. A tumoural angiogenic gateway blocker, Benzophenone-1B represses the HIF-1 α nuclear translocation and its target gene activation against neoplastic progression. *Biochem Pharmacol.* 2017;125:26–40.
24. Prabhakar BT, Khanum SA, Shashikanth S, Salimath BP. Antiangiogenic effect of 2-benzoyl–phenoxy acetamide in EAT cell is mediated by HIF-1 α and down regulation of VEGF of in-vivo. *Invest New Drugs.* 2006;24:471–8.
25. Prabhakar BT, Khanum SA, Jayashree K, Salimath BP, Shashikanth S. Anti-tumor and proapoptotic effect of novel synthetic benzophenone analogues in Ehrlich ascites tumor cells. *Bioorganic Med Chem.* 2006;14:435–46.
26. Maj E, Papiernik D, Wietrzyk J. Antiangiogenic cancer treatment: The great discovery and greater complexity. *Int J Oncol.* 2016;49:1773–84.
27. Xu D, Xu Z. Indole Alkaloids with potential anticancer activity. *Curr Top Med Chem.* 2020;20:1938–49.
28. Mohammed YH, Thirusangu P, Vigneshwaran V, Prabhakar BT, Khanum SA. The anti-invasive role of novel synthesized pyridazine hydrazide appended phenoxy acetic acid against neoplastic development targeting matrix metallo proteases. *Biomed Pharmacother.* 2017;95:375–86.
29. Chung AS, Lee J, Ferrara N. Targeting the tumour vasculature: insights from physiological angiogenesis. *Nat Rev Cancer.* 2010;10:505–14.
30. Rogers MS, Birsner AE, D’amato RJ. The mouse cornea micro-pocket angiogenesis assay. *Nat Protoc.* 2007;2:2545–50.
31. Shivakumar S, Prabhakar BT, Jayashree K, Rajan MG, Salimath BP. Evaluation of serum vascular endothelial growth factor (VEGF) and microvessel density (MVD) as prognostic indicators in carcinoma breast. *J Cancer Res Clin Oncol.* 2009;135:627–36.